



RESEARCH LETTER

10.1002/2015GL065341

Special Section:

First Results from the MAVEN Mission to Mars

Key Points:

- Presentation of the MAVEN/IUVS observations of the Martian oxygen corona
- Derivation of the oxygen density and temperature at the exobase
- Observations of possible diurnal variations of the cold oxygen corona

Correspondence to:

J. Y. Chaufray,
chaufray@latmos.ipsl.fr

Citation:

Chaufray, J. Y., et al. (2015), Study of the Martian cold oxygen corona from the O I 130.4 nm by IUVS/MAVEN, *Geophys. Res. Lett.*, 42, doi:10.1002/2015GL065341.

Received 12 JUL 2015

Accepted 11 SEP 2015

Study of the Martian cold oxygen corona from the O I 130.4 nm by IUVS/MAVEN

J. Y. Chaufray¹, J. Deighan², M. S. Chaffin², N. M. Schneider², W. E. McClintock², A. I. F. Stewart², S. K. Jain², M. Crismani², A. Stiepen², G. M. Holsclaw², J. T. Clarke³, F. Montmessin¹, F. G. Eparvier², E. M. B. Thiemann², P. C. Chamberlin⁴, and B. M. Jakosky²¹LATMOS-IPSL, CNRS, UVSQ, UMPC, Guyancourt, France, ²LASP, University of Colorado Boulder, Boulder, Colorado, USA, ³Center for Space Physics, Boston University, Boston, Massachusetts, USA, ⁴NASA Goddard Space Flight Center, Greenbelt, Maryland, USA

Abstract First observations of the O I 130.4 nm resonant line performed by the Imaging Ultraviolet Spectrograph (IUVS) aboard the Mars Atmosphere and Volatile Evolution mission (MAVEN) are presented in this paper. This emission line is observed during the different orbit phases of MAVEN. The atomic oxygen density and the temperature at 200 km are retrieved from an automatic pipeline using a radiative transfer model for resonant scattering lines for a selection of coronal profiles. These selected profiles are representative of the coronal scans done during the first months of the mission (from November 2014 to January 2015). The derived oxygen density and the temperature near the exobase are in the predicted range by the current thermospheric models of Mars for moderate solar activity, and some diurnal variations are observed. However, the absolute calibration of the instrument significantly limits the accuracy of density and temperature results.

1. Introduction

The Mars Atmosphere and Volatile Evolution mission (MAVEN) was inserted into orbit around Mars in September 2014. This mission is motivated by the study of the Mars atmospheric erosion rates along its history [Jakosky et al., 2015]. Atmospheric erosion primarily occurs in the upper atmosphere, and therefore, the understanding of the energetics, chemistry, and dynamics of the Martian upper atmosphere is crucial to constrain the contribution of the different escape channels to the Martian atmospheric erosion [Bougher et al., 2014]. Atomic oxygen, produced by photodissociation of the atmospheric carbon dioxide, becomes the main neutral species in the upper thermosphere and the low exosphere of Mars (~200–500 km) [Nier and McElroy, 1977; Barth et al., 1992]. This species is important for several processes in the Martian upper atmosphere. For example, atomic oxygen and carbon dioxide collisions can excite the v_2 vibrational state of CO₂ that regulates the Martian temperature at the exobase. This vibrational state, which increases the 15 μ m emission, leads to a high thermospheric cooling rate [López-Puertas et al., 1992; Bougher et al., 1999; Gonzalez-Galindo et al., 2005, 2009; Huestis et al., 2008]. The Martian ionosphere is mainly composed of O₂⁺, CO₂⁺, and O⁺ whose abundances are chemically controlled by the amount of atomic oxygen in the thermosphere [Hanson et al., 1977; Gonzalez-Galindo et al., 2013; Chaufray et al., 2014; Bougher et al., 2015]. Dissociative recombination of O₂⁺ is an important source of oxygen escape [e.g., McElroy, 1972; Chaufray et al., 2007; Kaneda et al., 2009; Fox and Hac, 2014; Gröller et al., 2014] with important seasonal variations [Vaille et al., 2009; Yagi et al., 2012; Lee et al., 2015]. According to recent global circulation models (GCMs) simulations, cold atomic oxygen is very sensitive to the thermospheric circulation, and its expected diurnal variations could constrain the dynamics of the Martian upper atmosphere [Vaille et al., 2009; Gonzalez-Galindo et al., 2009; Bougher et al., 2015]. Moreover, exospheric oxygen can be ionized and picked up by the solar wind contributing to the atmospheric escape [Lundin et al., 2008]. Therefore, it is important to know the thermospheric/exospheric oxygen density and its variability to understand the Martian environment from the thermosphere to the magnetosphere.

The first observations of the 130.2, 130.5, and 130.6 nm resonance triplet transitions of atomic oxygen (referred to as O 130.4 nm line) on Mars were made during the two flybys of Mariner 6 and Mariner 7 (31 July 1969 and 5 August 1969). These observations were performed during a period of high solar activity (solar radio flux at 10.7 cm $F_{10.7} = 167$ –188 solar flux units (sfu)) for a solar longitude $L_s = 200^\circ$ (Martian year 8) slightly after the northern autumn equinox [Barth et al., 1971]. Extensive observations were performed later

by Mariner 9 from November 1971 to October 1972 [Barth, 1974] during a period of moderate solar activity ($F_{10.7} = 110\text{--}140$ sfu) from $L_s \sim 290^\circ$ (Martian year 9) to $L_s \sim 100^\circ$ (Martian year 10). The brightness of the emission was typically between 0.1 and 1 kR at between 100 and 400 km. Strickland *et al.* [1972] derived a [O]/[CO₂] mixing ratio of $\sim 0.5\text{--}1\%$ at 1.2 nbar (~ 135 km). The best fit was obtained with a solar O I triplet of 6×10^9 ph/cm²/s at 1 AU and a photoelectron excitation frequency of 1.5×10^{-8} s⁻¹. The fits were performed for three typical temperature values (300, 350, and 435 K) encompassing the value derived from Lyman- α observations [Anderson and Hord, 1971]. These results showed that the resonant scattering is the main source for the 130.4 nm emission line on Mars. Using the larger set of limb and disk observations carried out by Mariner 9, Strickland *et al.* [1973] confirmed the main results derived from Mariner 6 and 7 observations, using a revised value of the photoelectron excitation frequency of 3.6×10^{-8} s⁻¹.

Furthermore, they found that O I 130.4 nm emission was mainly produced by solar resonant scattering. Disk data show large local time/aerographical variations of the oxygen density with a larger density in the afternoon relative to the morning. The Mariner 9 observations were reanalyzed later by Stewart *et al.* [1992] and compared to the Martian Thermospheric GCM (MTGCM) of the University of Michigan [Bougher *et al.*, 1990]. The predicted brightness by the MTGCM showed a slightly lower overall level than the data within the calibration uncertainty. The larger 130.4 nm solar flux and photoelectron impact cross section led Stewart *et al.* [1992] to derive lower amount of oxygen compared to Strickland *et al.* [1973] due to a larger 130 nm solar flux and photoelectron impact cross section. This study confirmed the afternoon/morning brightness asymmetry reported in Strickland *et al.* [1973]. This afternoon/morning asymmetry was not reproduced by the MTGCM of Bougher *et al.* [1990].

Stewart *et al.* [1992] also noticed an increase of the oxygen abundance in the southern hemisphere, in contrast with the MTGCM predictions of high densities in the winter (northern) hemisphere. The authors pointed out that waves activity, as observed by the Viking entry data, could strongly affect the Martian upper atmosphere as they do on Earth. This wave activity could have been triggered by the global dust storm just prior to the arrival of Mariner 9 at Mars. Recent GCM simulations have confirmed the strong impact of the global dust storms on the Martian thermospheric and mesospheric circulation [Medvedev and Yigit, 2012].

The Spectroscopy for Investigation and Characteristics of the Atmosphere of Mars (SPICAM)-UV aboard Mars Express performed observation of the 130.4 nm O I line from October 2004 to February 2005. Chaufray *et al.* [2009] analyzed these data that were acquired during a period of low solar activity suggesting that the resonance scattering is the dominant source of excitation. Oxygen density $\sim 0.7\text{--}2.4 \times 10^7$ cm⁻³ at 200 km was derived from these observations. Exospheric temperatures of ~ 300 K higher than the ~ 200 K expected from CO₂⁺ doublet at 289 nm analysis [Leblanc *et al.*, 2006] and from Krasnopolsky [2002] for low solar activity better reproduced the observations. The main source of uncertainty was the absolute calibration as expected for an optically thick emission.

The oxygen density vertical profile derived during the Mars flyby of the Rosetta spacecraft from the O I 130.4 nm by the Ultraviolet Imaging Spectrometer Alice [Feldman *et al.*, 2011] showed for the first time the presence of a hot oxygen population confirming previous theoretical studies [McElroy, 1972] and independent measurements from the Space Telescope Imaging Spectrograph (STIS) aboard Hubble Space Telescope (HST) [Carveth *et al.*, 2012]. This hot oxygen population was dominant above ~ 500 km. The cold oxygen population dominant below 500 km was in agreement with an oxygen density of 3×10^7 cm⁻³ and a temperature of 200 K at 200 km, though not well constrained because of the coarse spatial resolution of the brightness profile [Feldman *et al.*, 2011].

2. Observations

The Imaging Ultraviolet Spectrograph (IUVS) is described in detail in McClintock *et al.* [2015]. It works with two different modes: a "normal" mode providing broad spectra (120–330 nm) with a moderate resolution ($R \sim 200$) and an echelle mode providing only few emission lines from H and D (Lyman- α) and from O (130.4 nm triplet). The echelle mode has a sufficient spectral resolution ($R = 14,500$) to separate the three lines of the O I 130.4 nm triplet. Observations of the O I 130.4 nm triplet using the echelle mode will be presented in a future work. For the normal mode, a beam splitter transmits wavelengths greater than 180 nm to the

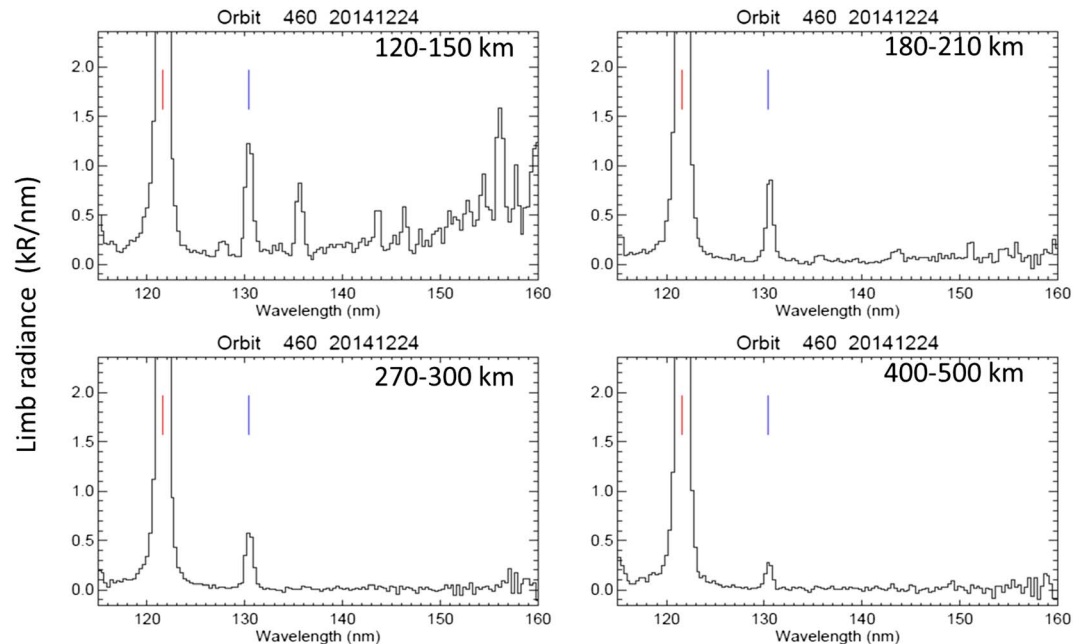


Figure 1. Examples of IUVS spectra obtained during an orbit side phase (outbound) during orbit 460 (24 December 2014; $L_s = 259$). These spectra correspond to averages of individual spectra over an altitude range of (top left) 120–150 km, (top right) 180–210 km, (bottom left) 270–300 km, and (bottom right) 400–500 km. The red and blue vertical lines indicate the position of the H 121.6 nm and the O 130.4 nm lines.

middle ultraviolet detector and wavelengths shorter than 180 nm to the far ultraviolet (FUV) detector. The OI 130.4 nm is therefore observed on the FUV detector.

IUVS observations are organized by orbit phase “periapsis,” “apoapsis,” and “orbit sides” separated in “outbound” and “inbound” phases [McClintock *et al.*, 2015]. These names are used as filename identifiers. The OI 130.4 nm emission is observed during all the phases except during the inbound phase. During typical periapsis limb scans, 12 scans are done at different solar zenith angles. The OI 130.4 nm emission line is observed from ~ 100 km to ~ 250 km with a spatial resolution of ~ 5 km. During the apoapsis phase, the OI 130.4 nm is mainly observed over the Martian disk. During the outbound phase, the OI 130.4 nm emission is observed from the disk to the exosphere. The last phase is the best phase to study the vertical profile of the OI 130.4 nm emission over a large altitude range.

Four spectra observed by IUVS during the outbound phase at different altitudes are presented in Figure 1. At altitudes lower than 150 km, several lines are observed, including the H Lyman- α and O 130.4 nm. The CO Fourth Positive band associated with the C atomic line at 156.5 nm and O 135.6 nm line are observed as previously observed by several instruments [e.g., Barth *et al.*, 1971; Feldman *et al.*, 2000; Leblanc *et al.*, 2006]. As observed with SPICAM/MEX, above 180 km, the resonant lines of the hydrogen at 121.6 nm (see Chaffin *et al.* [2015]) and the oxygen at 130.4 nm are the only emission lines observed in the FUV range [Chaufray *et al.*, 2009; Futaana *et al.*, 2011]. The O line at 135.6 nm is a forbidden line produced by photoelectron impact on O. This emission is optically thin, and its brightness is characterized by a small-scale height compared to the O 130.4 optically thick line. Above 300 km, the OI 130.4 nm brightness decreases sharply but, contrary to SPICAM, is still observed at 500 km indicating a better sensitivity of IUVS compared to SPICAM in this wavelength range.

The brightness of the O 130.4 nm line is computed by spectral integration assuming a residual linear background from the calibrated (level 1b) IUVS/MAVEN data.

Examples of OI 130.4 nm brightness observed from the three phases as well as an observation performed during the 35 h insertion orbit are presented in Figure 2, illustrating the diversity and complementarity of the IUVS observations of the O 130.4 nm line. The brightness of the line decreases with solar zenith angle (SZA) as observed in Figures 2a–2c. The emission is generally not detected for $SZA > 110^\circ$. The absolute

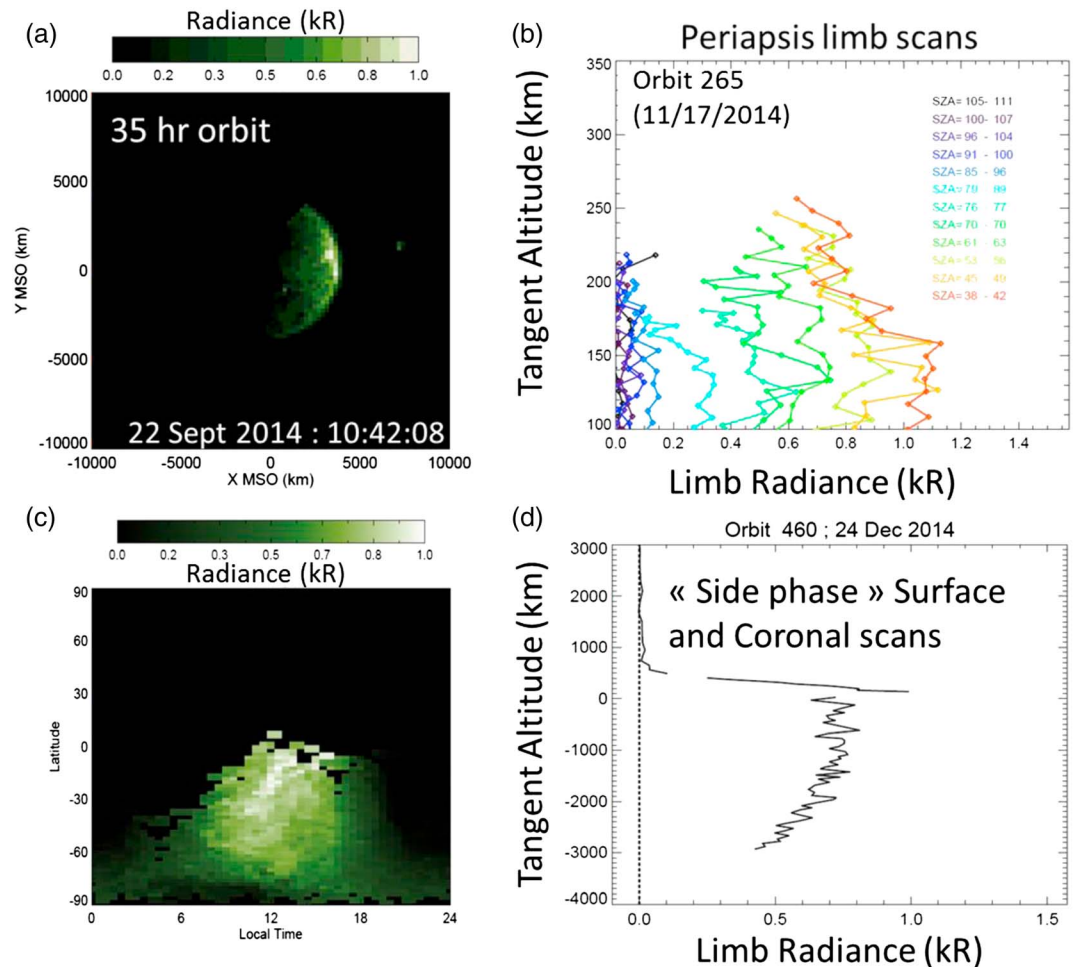


Figure 2. Different observations of the O I 130.4 nm emission performed by IUVS during the first months of observations. (a) Mars observation performed during the 35 h insertion orbit (22 September 2014 at 10:42:08) projected into X-Y (Mars solar orbit) MSO axis: The sun is on x axis, on the right. (b) Examples of the 12 limb scans performed at periapsis during the MAVEN orbit 265 (17 November 2014) at different solar zenith angles (at the impact point). (c) Cylindrical projection of the disk brightness observation at apoapsis during the MAVEN orbit 426 (18 December 2014) represented in local time/latitude map. (d) Example of surface and coronal scans obtained during the “orbit side: outbound” phase of the orbit 460 (24 December 2014) of MAVEN. For Figures 2b and 2d, the altitude is the altitude of the impact point.

brightness observed by IUVS is larger than the brightness derived from SPICAM/Mars Express observations by a factor of ~1.6. When taking into account the solar flux at Mars, this factor is reduced to 1.3. This difference could be due to the absolute calibration of both instruments or to a difference in the oxygen content of the Martian upper atmosphere due to the different solar activity and season. The brightness is in better agreement with Mariner 6 and 9 observations [Strickland *et al.*, 1972; Stewart *et al.*, 1992], as well as HST/STIS observations done in 2003 [Carveth *et al.*, 2012] and 2014.

The bright limb near 150 km is visible from periapsis and outbound side observations (Figures 2b and 2d). Such a bright limb has been observed from the very thick optical emissions [Gladstone, 1988] and attributed to the effect of the wings of the scattering cross section. Indeed, while the spectral core of the line is optically thick and should not produce a bright limb, the wings are optically thin and produce the observed bright limb. This bright limb was not clearly seen from SPICAM/Mars Express due to the contamination by stray light at altitudes lower than 150 km [Leblanc *et al.*, 2006; Chaufray *et al.*, 2009] or from HST probably because of the lower spatial resolution. The O I 130.4 nm is visible at SZA < 110° (Figures 2a and 2b), and the brightness at the dayside for SZA < 60° is typically between 0.8 and 1.2 kR as seen from the different mode of observations.

This paper is primarily focused on the method used to derive the oxygen density from the O I 130.4 nm resonance line using the “normal grating,” and it reports on the outbound phase observations. However, the derivation could be applied to the other orbit phase observations keeping in mind the limits of the method described below, especially the 1-D assumption when studying the disk observations. In this paper, we will focus on the optically thick emission line associated with the cold corona; the hot oxygen population is studied by *Deighan et al.* [2015].

3. Oxygen Density and Temperature Derivation

3.1. General Method

To derive the oxygen density and the temperature at the exobase, we use a forward approach similar to *Chaufray et al.* [2009], neglecting the photoelectron impact excitation. The photoelectron impact excitation source has been estimated from previous studies to contribute only few percentages to the total brightness [*Strickland et al.*, 1972, 1973; *Chaufray et al.*, 2009]. The effects of the photoelectron impact on the derived parameters (oxygen density and temperature) could be estimated from the sensitivity study performed in the next section.

For the forward inversion approach, the one-dimensional (1-D) oxygen density profile is divided into two parts: a thermospheric profile from 80 to 200 km and an exospheric profile from 200 to 1000 km. The O and CO₂ thermospheric profiles are calculated by solving the coupled diffusion and hydrostatic equations [*Hunten*, 1973]. In this region, the temperature and eddy mixing coefficients profiles are taken from *Krasnopolsky* [2002]. The CO₂ density at 80 km is chosen to be $2.6 \times 10^{13} \text{ cm}^{-3}$ [*Krasnopolsky*, 2002] in good agreement with the average value estimated from stellar occultations by SPICAM [*Forget et al.*, 2009]. Above the exobase, we use a 1-D Chamberlain approach to describe the oxygen exospheric density [*Chamberlain*, 1963]. We neglect the hot oxygen component in this study. The simulated cold O density from 80 to 1000 km is fully determined knowing the temperature at the exobase and the density at a given altitude (here at 80 km).

The O I emission volume rate from solar photons resonant scattering is computed for each O density profiles using an updated version of the radiative transfer model used by *Chaufray et al.* [2009]. This new version takes into account the natural broadening of the absorption cross section. One hundred models of the emission volume rate (10 values of the exospheric temperatures from 175 to 400 K with a 25 K step and 10 values of the oxygen density at 80 km from 10^9 to 10^{12} cm^{-3} with a constant multiplicative step ~ 2.15) have been computed.

For this analysis, the solar flux at 130.4 nm is taken from Extreme Ultraviolet Monitor (EUVM)/MAVEN [*Eparvier et al.*, 2015]. The solar flux, rescaled to 1 AU, is $\sim 1.1\text{--}1.2 \times 10^{14} \text{ ph/m}^2/\text{nm}$ during the first months of observations by MAVEN. We assume that all the solar flux between 130 and 131 nm is due to the solar oxygen triplet and use the solar spectral shape derived by *Gladstone* [1992].

A Levenberg-Marquardt procedure is then used to derive the value of the two free parameters minimizing a χ^2 function [*Gill et al.*, 1981]. In this procedure, the expected brightness is computed from a first guess of these parameters taking into account the geometry of the observations (spacecraft position and line of sight direction). This procedure is used to iteratively find the values leading to the χ^2 minimization. This procedure is not sensitive to the first guess.

The typical time needed to derive the two parameters (oxygen density at 80 km and temperature at 200 km) from one observation is ~ 5 min, making the procedure useful for a systematic study of all the outbound phase observations. The oxygen density at 200 km is then derived by interpolation.

The procedure can be applied for any kind of observations, but the 1-D assumption is better suited for scan limbs than disk observations due to the expected local time and latitude variations of both oxygen density and temperatures [e.g., *Vaille et al.*, 2009; *Gonzalez-Galindo et al.*, 2009; *Bougher et al.*, 2015]. A 3-D parametrized model will lead to too many free parameters, making impossible a systematic retrieval of the oxygen density from one observation to another. In this paper, we will focus on the limb scan part of the outbound profiles. Such an approach has been used in the past to study Mariner's and Mars Express observations providing almost all the current information on the atomic oxygen in the Martian upper atmosphere [*Stewart et al.*, 1992; *Chaufray et al.*, 2009].

Table 1. Sensitivity of the Derived Parameters to the IUVS Absolute Calibration

Scale Parameter	Oxygen Density at 200 km	Temperature at 200 km
0.75	$9.8 \times 10^6 \text{ cm}^{-3}$	347 K
0.85	$1.7 \times 10^7 \text{ cm}^{-3}$	326 K
0.95	$2.9 \times 10^7 \text{ cm}^{-3}$	308 K
1.05	$4.6 \times 10^7 \text{ cm}^{-3}$	290 K
1.15	$6.4 \times 10^7 \text{ cm}^{-3}$	289 K
1.25	$8.2 \times 10^7 \text{ cm}^{-3}$	287 K

3.2. Sensitivity to Absolute Calibration

IUVS was calibrated against UV-bright stars and scaled by instrument geometric factors appropriate for extended source observations. The uncertainty on the absolute calibration is estimated to be $\pm 25\%$. In this section, we investigate the sensitivity of the derived parameters (oxygen density and temperature at the

exobase) to the absolute calibration of IUVS, using a scaling factor from 0.75 to 1.25 to take into account the calibration uncertainty [Schneider *et al.*, 2015]. The oxygen density and temperature at 200 km derived from the observation during orbit 460 for different values of the scaling factor are given in Table 1.

As expected from an optically thick emission, these two parameters are very sensitive to the absolute calibration of the instrument. If the brightness is rescaled by a factor of 0.75, the oxygen density at 200 km decreases by a factor of ~ 4 . For an optically thick emission, the scale height of the brightness is controlled by both temperature and density. Therefore, a decrease of the oxygen density is associated with an increase of the temperature to reproduce the observed brightness scale height. If the absolute brightness is rescaled by 0.75, the derived temperature increases by 20% to ~ 350 K. If the brightness is

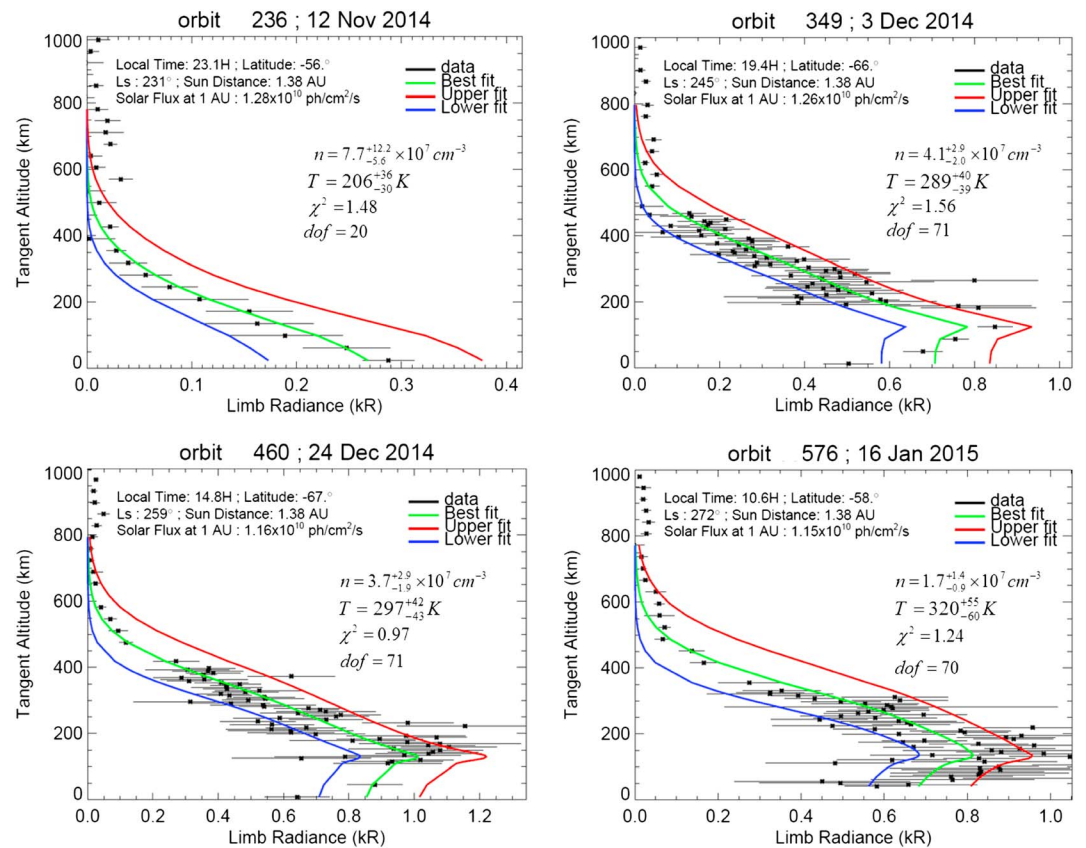


Figure 3. Examples of coronal scan limb profiles during the side phase of the orbit of MAVEN. The observed brightness profile (black dots) associated with a statistical error bar (black lines) derived from the different spatial bins along the slit is compared to the best fit (green line) derived from the method described in section 3. The upper (lower) fit represents the brightness profile obtained using the upper (lower) value of the derived temperature and oxygen density at the exobase (red and blue lines). The value of the reduced chi-square, the degree of freedom (dof), and number of lines of sight minus the two free parameters are also indicated.

rescaled by a factor of 1.25, the oxygen density at 200 km increases by a factor of ~ 2 , while the derived temperature decreases by only a few percent. For all the cases presented in Table 1, the values of the reduced χ^2 function for the best fit are between 0.9 and 1.

4. Results and Discussion

Examples of fits are displayed in Figure 3. Local time and latitude are those of the tangent point of the line of sight. These observations are representative of several observations done using a similar geometry and not presented here.

For these observations one part of the limb scan was done with a better spatial resolution using a small integration time in order to better catch the bright limb (orbits 460 and 576), but for some early observations (until orbit 420), due to timing problems, the scans occurred too early (e.g., orbit 236) or too late (e.g., orbit 349). This implies a low signal-to-noise ratio for one individual spectrum leading to the scattering on the displayed data.

The detailed analysis of the full set of observations is deferred to a future paper. The results obtained from this limited set of observations are representative of the first observations from November 2014 to January 2015, starting slightly before and ending slightly after the Martian perihelion ($L_s = 251^\circ$). The observed bright limb (orbits 349, 460, and 576) is reasonably reproduced by the model when the natural broadening and therefore the extended spectral wings of the scattering cross sections are taken into account as discussed in the previous section. No bright limb is observed at the nightside (orbit 236) as expected from radiative transfer simulations. The temperature and oxygen density are found in the range predicted by GCMs [Gonzalez-Galindo *et al.*, 2009; Bougher *et al.*, 2015] $\sim 10^7\text{--}10^8\text{ cm}^{-3}$ and 200–300 K for moderate solar activity and consistent with dayglow analysis $325 \pm 25\text{ K}$ for local time near 14:00 [Evans *et al.*, 2015]. The exospheric temperature is generally lower at the nightside (orbit 236) than at the dayside (orbits 349, 460, and 576), which is expected and due to the EUV heating at the dayside. There is a slight difference in the oxygen density derived from orbits 460 and 576 for a similar exospheric temperature. This possible local time variation of the oxygen density, similar to the morning/afternoon asymmetry observed from Mariner 9 [Stewart *et al.*, 1992], could also be due to shorter time scale variations.

5. Summary and Conclusion

A first set of representative observations of the O I 130.4 nm by IUVS/MAVEN is presented, and the first coronal limb scans are used to derive the atomic oxygen content in the Martian upper atmosphere. The derived parameters (oxygen density and temperature at 200 km) are very sensitive to the absolute calibration. The first trends derived from a limited set of observations are in good agreement with the trends derived from Mariner 9 mission. From the full current set and future observations of the O I 130.4 nm, we could expect to produce a better latitude, local time, and solar longitude coverage leading to the first atomic oxygen climatology complementary to and independent of the oxygen density retrieved from the Neutral Gas and Ion Mass Spectrometer [Mahaffy *et al.*, 2014]. The ultimate goal of the oxygen climatology is to better understand the dynamics and aeronomy of Mars comparing those measurements to the 3-D GCM [Gonzalez-Galindo *et al.*, 2013; Bougher *et al.*, 2015].

References

- Anderson, D. E., Jr., and C. W. Hord (1971), Mariner 6 and 7 ultraviolet spectrometer experiment: Analysis of hydrogen Lyman-alpha data, *J. Geophys. Res.*, *76*, 6666–6673, doi:10.1029/JA076i028p06666.
- Barth, C. A. (1974), The atmosphere of Mars, *Annu. Rev. Earth Planet. Sci.*, *2*, 333–367.
- Barth, C. A., C. W. Hord, J. B. Pearce, K. K. Kelly, G. P. Anderson, and A. I. Stewart (1971), Mariner 6 and 7 ultraviolet spectrometer experiment: Upper atmosphere data, *J. Geophys. Res.*, *76*, 2213–2227, doi:10.1029/JA076i010p02213.
- Barth, C. A., A. I. F. Stewart, S. W. Bougher, D. M. Hunten, S. J. Bauer, and A. F. Nagy (1992), Aeronomy of the current Martian atmosphere, in *Mars*, edited by H. H. Kieffer *et al.*, pp. 1054–1089, Univ. of Ariz. Press, Tucson.
- Bougher, S. W., R. G. Roble, E. C. Ridley, and R. E. Dickinson (1990), The Mars thermosphere: 2. General circulation with coupled dynamics and composition, *J. Geophys. Res.*, *95*, 14,811–14,827, doi:10.1029/JB095iB09p14811.
- Bougher, S. W., S. Engel, R. G. Roble, and B. Foster (1999), Comparative terrestrial planetary thermospheres. 2. Solar cycle variation of global structure and winds at equinox, *J. Geophys. Res.*, *104*, 16,591–16,611, doi:10.1029/1998JE001019.
- Bougher, S. W., T. E. Cravens, J. Grebowsky, and J. Luhmann (2014), The aeronomy of Mars: Characterization by MAVEN of the upper atmosphere reservoir that regulates volatile escape, *Space Sci. Rev.*, doi:10.1007/s11214-014-0053-7.

Acknowledgments

This work and the MAVEN project are supported by NASA through the Mars Exploration Program. The data used (all IUVS data tagged “early,” “out-bound,” “apoapse,” and “periapse” with revision/version tag v02_r01 and EUVM level 3 data) are archived in NASA’s Planetary Data System http://atmos.nmsu.edu/data_and_services/atmospheres_data/MAVEN/maven_iuvs.html. Thanks are owed to the many engineers on the MAVEN team who worked to enable observations of the corona within hours of the spacecraft’s arrival. J.-Y. Chaufray is supported by the Centre National d’Etudes Spatiales. A. Stiepen is supported by the Belgian American Educational Foundation and the Rotary District 1630. We thank S.W. Bougher and an anonymous reviewer for their useful comments to improve this paper.

The Editor thanks Stephen Bougher and an anonymous reviewer for their assistance in evaluating this paper.

- Bougher, S. W., D. Pawlowski, J. M. Bell, S. Nelli, T. McDunn, J. R. Murphy, M. Chizek, and A. Ridley (2015), Mars Global Ionosphere-Thermosphere Model: Solar cycle, seasonal, and diurnal variations of the Mars upper atmosphere, *J. Geophys. Res. Planets*, *120*, 311–342, doi:10.1002/2014JE004715.
- Carveth, C., J. T. Clarke, J.-Y. Chaufray, and J.-L. Bertaux (2012), Analysis of HST spatial profiles of oxygen airglow from Mars, B.A.A.S.
- Chaffin, M. S., et al. (2015), Three-dimensional structure in the Mars H corona revealed by IUVS on MAVEN, *Geophys. Res. Lett.*, *42*, doi:10.1002/2015GL065287.
- Chamberlain, J. W. (1963), Planetary coronae and atmospheric evaporation, *Planet. Space Sci.*, *11*, 901.
- Chaufray, J.-Y., R. Modolo, F. Leblanc, G. Chanteur, R. E. Johnson, and J. G. Luhmann (2007), Mars solar wind interaction: Formation of the Martian corona and atmospheric loss to space, *J. Geophys. Res.*, *112*, E09009, doi:10.1029/2007JE002915.
- Chaufray, J.-Y., F. Leblanc, E. Quémerais, and J.-L. Bertaux (2009), Martian oxygen density at the exobase deduced from O I 130.4 nm observations by SPICAM on Mars Express, *J. Geophys. Res.*, *114*, E02006, doi:10.1029/2008JE003130.
- Chaufray, J.-Y., F. Gonzalez-Galindo, F. Forget, M. Lopez-Valverde, F. Leblanc, R. Modolo, S. Hess, M. Yagi, P.-L. Blelly, and O. Witasse (2014), 3D Martian ionosphere model: II. Effect of transport processes due to pressure gradients, *J. Geophys. Res. Planets*, *119*, 1614–1636, doi:10.1002/2013JE004551.
- Deighan, J., et al. (2015), MAVEN IUVS observation of the hot oxygen corona at Mars, *Geophys. Res. Lett.*, *42*, doi:10.1002/2015GL065487.
- Eparvier, F. G., P. C. Chamberlain, T. N. Woods, and E. M. B. Thiemann (2015), The solar extreme ultraviolet monitor for MAVEN, *Space Sci. Rev.*, doi:10.1007/s11214-015-0195-2.
- Evans, J. S., et al. (2015), Retrieval of CO₂ and N₂ in the Martian thermosphere using dayglow observations by IUVS on MAVEN, *Geophys. Res. Lett.*, *42*, doi:10.1002/2015GL065489.
- Feldman, P. D., E. B. Burgh, S. T. Durrance, and A. F. Davidsen (2000), Far-ultraviolet spectroscopy of Venus and Mars at 4 Å resolution with the Hopkins Ultraviolet Telescope on Astro-2, *Astrophys. J.*, *538*, 395–400.
- Feldman, P. D., et al. (2011), Rosetta-Alice observations of exospheric hydrogen and oxygen on Mars, *Icarus*, *214*, 394–399.
- Forget, F., F. Montmessin, J.-L. Bertaux, F. Gonzalez-Galindo, S. Lebonnois, E. Quémerais, A. Réberac, E. Dimarellis, and M. A. Lopez-Valverde (2009), Density and temperatures of the upper Martian atmosphere measured by stellar occultations with Mars Express SPICAM, *J. Geophys. Res.*, *114*, E01004, doi:10.1029/2008JE003086.
- Fox, J. L., and A. B. Hac (2014), The escape of O from Mars: Sensitivity to the elastic cross sections, *Icarus*, *228*, 375–385.
- Futaana, Y., J.-Y. Chaufray, H. T. Smith, P. Garnier, H. Lichtenegger, M. Delva, H. Gröller, and A. Mura (2011), Exospheres and energetic neutral atoms of Mars, Venus and Titan, *Space Sci. Rev.*, *162*, 213–266, doi:10.1007/s11214-011-9834-4.
- Gill, P. R., W. Murray, and M. H. Wright (1981), The Levenberg-Marquardt method, in *Practical Optimization*, chap. 4.7.3, pp. 136–137, Academic, London.
- Gladstone, G. R. (1988), UV resonance line dayglow emission on Earth and Jupiter, *J. Geophys. Res.*, *93*, 14,623–14,630, doi:10.1029/JA093iA12p14623.
- Gladstone, G. R. (1992), Solar O I 1304-A triplet line profiles, *J. Geophys. Res.*, *97*, 19,519–19,525, doi:10.1029/92JA00991.
- Gonzalez-Galindo, F., M. A. Lopez-Valverde, M. Angelats i Coll, and F. Forget (2005), Extension of a Martian general circulation model to thermospheric altitudes: UV heating and photochemical models, *J. Geophys. Res.*, *110*, E09008, doi:10.1029/2004JE002312.
- Gonzalez-Galindo, F., F. Forget, M. A. López-Valverde, M. Angelats i Coll, and E. Millour (2009), A ground-to-exosphere Martian circulation model: 1. Seasonal, diurnal and solar cycle variation of thermospheric temperatures, *J. Geophys. Res.*, *114*, E04001, doi:10.1029/2008JE003246.
- Gonzalez-Galindo, F., J.-Y. Chaufray, M. A. López-Valverde, G. Gilli, F. Forget, F. Leblanc, R. Modolo, S. Hess, and M. Yagi (2013), 3D Martian ionosphere model: I. The photochemical ionosphere below 180 km, *J. Geophys. Res. Planets*, *118*, 2105–2123, doi:10.1002/jgre.20150.
- Gröller, H., H. Lichtenegger, H. Lammer, and V. J. Shematovich (2014), Hot oxygen and carbon escape from the martian atmosphere, *Planet. Space Sci.*, *98*, 93–105, doi:10.1016/j.pss.2014.01.007.
- Hanson, W. B., S. Satani, and D. R. Zuccaro (1977), The Martian ionosphere as observed by the Viking retarding potential analyzers, *J. Geophys. Res.*, *82*, 4351–4363, doi:10.1029/J5082i028p04351.
- Huestis, D. L., S. W. Bougher, J. L. Fox, M. Galand, R. E. Johnson, J. I. Moses, and J. C. Pickering (2008), Cross sections and reaction rates for comparative planetary aeronomy, *Space Sci. Rev.*, *139*, 63–105, doi:10.1007/s11214-008-9383-7.
- Hunten, D. M. (1973), The escape of light gases from planetary atmospheres, *J. Atmos. Sci.*, *30*, 1481–1494.
- Jakosky, B. M., et al. (2015), The Mars Atmosphere and Volatile Evolution (MAVEN) mission, *Space Sci. Rev.*, doi:10.1007/s11214-015-0139-x.
- Kaneda, K., N. Terada, and S. Machida (2009), Solar wind control of the hot oxygen corona around Mars, *J. Geophys. Res.*, *114*, E02007, doi:10.1029/2008JE003234.
- Krasnopolsky, V. A. (2002), Mars' upper atmosphere and ionosphere at low, medium, and high solar activities: Implications for evolution of water, *J. Geophys. Res.*, *107*(E12), 5128, doi:10.1029/2001JE001809.
- Leblanc, F., J.-Y. Chaufray, J. Liliensten, O. Witasse, and J.-L. Bertaux (2006), Martian dayglow as seen by the SPICAM UV spectrograph on Mars Express, *J. Geophys. Res.*, *111*, E09S11, doi:10.1029/2005JE002664.
- Lee, Y., M. R. Combi, V. Tenishev, S. W. Bougher, J. Deighan, N. M. Schneider, W. E. McClintock, and B. Jakosky (2015), A comparison of 3D model predictions of Mars' oxygen corona with early MAVEN IUVS observations, *Geophys. Res. Lett.*, *42*, doi:10.1002/2015GL065291.
- López-Puertas, M., M. A. Lopez-Valverde, C. P. Rinsland, and M. R. Gunson (1992), Analysis of the upper atmosphere CO₂(ν₂) vibration temperatures retrieved from ATMOS-Spacelab 3 observations, *J. Geophys. Res.*, *97*, 20,469–20,478, doi:10.1029/92JD02026.
- Lundin, R. S., S. Barabash, M. Holmstrom, H. Nilsson, M. Yamauchi, M. Fraenz, and E. M. Dubinin (2008), A comet like escape of ionospheric plasma from Mars, *Geophys. Res. Lett.*, *35*, L18203, doi:10.1029/2008GL034811.
- Mahaffy, P. R., et al. (2014), The Neutral Gas and Ion Spectrometer on the Mars Atmosphere and Volatile Evolution Mission, *Space Sci. Rev.*, doi:10.1007/s11214-014-0091-1.
- McClintock, W. E., N. M. Schneider, G. M. Holsclaw, J. T. Clarke, A. C. Hsokins, I. Stewart, F. Montmessin, R. Yelle, and J. Deighan (2015), The Imaging Ultraviolet Spectrograph (IUVS) for the MAVEN mission, *Space Sci. Rev.*, doi:10.1007/s11214-014-0098-7.
- McElroy, M. B. (1972), Mars: An evolving atmosphere, *Science*, *175*, 443–445.
- Medvedev, A. S., and E. Yigit (2012), Thermal effects of internal gravity waves in the Martian thermosphere, *Geophys. Res. Lett.*, *39*, L05201, doi:10.1029/2012GL050852.
- Nier, A. O., and M. B. McElroy (1977), Composition and structure of Mars' upper atmosphere results from the neutral mass spectrometers on Viking 1 and 2, *J. Geophys. Res.*, *82*, 4341–4349, doi:10.1029/J5082i028p04341.
- Schneider, N. M., et al. (2015), MAVEN IUVS observations of the aftermath of the comet Siding Spring meteor shower on Mars, *Geophys. Res. Lett.*, *42*, 4755–4761, doi:10.1002/2015GL063863.

- Stewart, A. I. F., M. J. Alexander, R. R. Meier, L. J. Paxton, S. W. Bougher, and C. G. Fesen (1992), Atomic oxygen in the Martian thermosphere, *J. Geophys. Res.*, *97*, 91–102, doi:10.1029/91JA02489.
- Strickland, D. J., G. E. Thomas, and P. R. Sparks (1972), Mariner 6 and 7 ultraviolet spectrometer experiment: Analysis of the O I 1304 and 1356 A emissions, *J. Geophys. Res.*, *77*, 4052–4067, doi:10.1029/JA077i022p04052.
- Strickland, D. J., A. I. Stewart, C. A. Barth, and C. W. Hord (1973), Mariner 9 ultraviolet spectrometer experiment: Mars atomic oxygen 1304-A emission, *J. Geophys. Res.*, *78*, 4547–4559, doi:10.1029/JA078i022p04547.
- Vaille, A., V. Tenishev, S. W. Bougher, M. R. Combi, and A. F. Nagy (2009), Three-dimensional study of Mars upper thermosphere/ionosphere and hot oxygen corona: 1. General description and results at equinox for solar low conditions, *J. Geophys. Res.*, *114*, E11005, doi:10.1029/2009JE003388.
- Yagi, M., F. Leblanc, J.-Y. Chaufray, F. Gonzalez-Galindo, S. Hess, and R. Modolo (2012), Mars exospheric thermal and non-thermal components: Seasonal and local variations, *Icarus*, *221*, 682–693, doi:10.1016/j.icarus.2012.07.022.